DNS on turbulent heat transfer of viscoelastic fluid flow in a plane channel with transverse rectangular orifices

Takahiro Tsukahara*, Tomohiro Kawase, Yasuo Kawaguchi

Department of Mechanical Engineering, Tokyo University of Science, 2641 Yamazaki, Noda-shi, Chiba 278-8510 Japan

Abstract

Heat-transfer characteristics of a viscoelastic turbulence past rectangular orifices were investigated in the context of the reduction effects of fluid elasticity on drag and heat transfer. To simulate the fully-developed channel flow through transverse orifices located periodically at intervals of 6.4 times channel height, we imposed periodic conditions at the upstream and downstream boundaries. To discuss the dissimilarity between the velocity and thermal fields, the molecular Prandtl number was set to be 1.0 and any temperature dependence of the fluid and rheological properties was not considered. In the present condition, the ratio of the reduction rates in drag and heat transfer was found to be 2.8:1.0, revealing that the present flow configuration is better than a smooth channel for avoiding the heat-transfer reduction. This phenomenon was attributed to the sustainment of the quasi-streamwise vortex downstream of the reattachment point despite the absence of strong spanwise vortices emanating from the orifice edge in the viscoelastic fluid. The longitudinal vortices behind the reattachment point caused a high turbulent heat flux and increase the local Nusselt number.

Keywords: channel flow; direct numerical simulation (DNS); drag reduction; Giesekus model; immersed boundary method; Kelvin-Helmholtz

*Corresponding author

Email address: tsuka@rs.tus.ac.jp (Takahiro Tsukahara)

Please cite this article as: Tsukahara, T., Kawase, T., and Kawaguchi, Y., DNS on turbulent heat transfer of viscoelastic fluid flow in a plane channel with transverse rectangular orifices. Progress in Computational Fluid Dynamics, Vol. 13 (2013), 212–223. doi:10.1504/PCFD.2013.053662

instability; non-Newtonian fluid; orifice; rheology; dissimilarity of heat and momentum; Toms effect; turbulence control; turbulent heat transfer; viscoelastic fluid.

1. Introduction

Since turbulent drag reduction (DR) has major benefits in reducing energy consumption in a variety of industrial applications, many researchers have investigated drag-reducing technology. The addition of small amounts of long chain polymer molecules or surfactant additives to wall-bounded turbulent flows can suppress turbulence and lead to a dramatic DR. This phenomenon is the so-called Toms effect (Toms, 1948) and can be used for reducing the transportation power in oil-pipeline circuits or district heating and cooling (DHC) recirculation systems. In general, the solution used as a working fluid for such a drag-reduced flow is a viscoelastic liquid. However, methods to design a viscoelastic-fluid system are far from satisfactory, and there have been many studies on drag reduction using both experiments and simulation (for instance, Dimitropoulos *et al.*, 2001; Yu and Kawaguchi, 2004; White and Mungal, 2008; Cai *et al.*, 2009; Tsukahara *et al.*, 2011a; Motozawa *et al.*, 2012). As it is known to be a practical problem for heat transport systems, the Toms effect also reduces turbulent heat transfer due to the suppression of turbulent motions, causing a heat-transfer reduction (HTR). For instance, Gupta *et al.* (2005) and Yu and Kawaguchi (2005) provided the results of direct numerical simulations (DNSs) of passive scalar (heat) transport in turbulent viscoelastic-fluid flow in a channel. They revealed reduction in the wall-normal heat flux and enhancement in the streamwise one, as compared to Newtonian flow, occurred in the viscoelastic flow and these were attributed to the changes in the correlation between velocity and temperature fluctuations. This reduced heat-transfer behavior of the viscoelastic turbulent channel flow would be desirable for heat pumps to carry liquid in terms of adiabatic transport, but it should be an obstacle to their application in DHC systems since heat exchange in heating or cooling is essential. Recently, our groups (Kagawa *et al.*, 2008; Tsukahara and Kawaguchi, 2011b,c; Wang *et al.*, 2011) performed parametric studies for different rheological parameters, using DNS, to find a fluid property that gives rise to a high rate of DR but a low HTR rate. However, they commonly reported that the DR and the HTR were basically comparable in the smooth plane channel flow.

Separation and reattachment in turbulent flows are well-known to induce some dissimilarity between velocity and thermal fields, and they occur in many practical engineering applications: e.g., sudden expansion pipe flows, ribbed or roughened channel flows, backward-facing step flow, and so on. In particular, regularly spaced elements, that induce separation and reattachment, such a series of orifices and array of pin fins have been applied practically due to their excellent heat transfer performance, e.g., in cooling of electronic components, in cooling of gas turbine blades, and recently, in hot water boilers of DHC. Makino *et al.* (2008a,b) carried out DNS of the Newtonian-fluid turbulent flow in a channel with periodic two-dimensional orifices, and investigated the performance of the heat transfer behind the orifice. They reported several differences in turbulent statistics between the flow past the orifice and the backward-facing step flow. Recently, the authors' group investigated the viscoelastic fluid in a channel with the same rectangular orifice using DNS (Tsukahara *et al.*, 2011d,e). We have confirmed that the fluid elasticity affects on various turbulent motions in just downstream of the orifice and attenuates spanwise vortices. To the author's knowledge there has to date been no detailed numerical analysis on the modulation of scalar heat transport in the viscoelastic flow through complicated geometry.

In the present work, we have performed DNS of the turbulent heat transfer in a channel flow of the viscoelastic fluid with the orifices and investigated the influence of dissimilarity between heat and momentum transports caused by the separation and reattachment of the flow. To achieve a clearer picture of the roles of viscoelasticity and turbulence modulations on the heat transfer, we used the Giesekus' viscoelastic-fluid model without any temperature dependency and selected the unity Prandtl number and a moderate Weissenberg number. All fluid properties are considered constant so that the heat is treated as passive scalar and the buoyancy effect and the temperature dependence of the present results are neglected.

2. Numerical procedure

The configuration of the computational domain we considered here is shown in Figure 1. Periodically repeating spatial units of transverse two-dimensional orifices are simulated with the periodic boundary conditions in the streamwise (x) and the spanwise (z) directions.

The height of each rib is chosen as 0.5δ—the channel half height is δ—and thus the blockage ratio of the orifice is 1:2. These present conditions relating

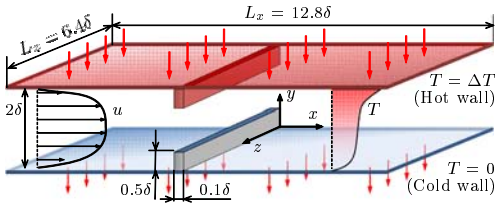

Figure 1: Configuration of the computational domain.

to orifice installation are the same as those studied by Makino *et al.* (2008a). The no-slip boundary condition is used on all the wall surfaces including the faces of the orifice. The main flow is driven by the streamwise mean pressure gradient. As for the thermal boundary condition, a constant temperature difference between the top and bottom walls ($\Delta T = \text{Const.}$) is imposed.

In this study, we restrict the discussion to incompressible flow and passive scalar (heat) transport for which the governing equations for the three velocity components $\mathbf{u} = \{u, v, w\}$, pressure p, additional stress-tensor component $\boldsymbol{\tau}_\mathrm{p}$ due to additives in the viscoelastic-fluid solution, and temperature T are

$$\nabla \cdot \mathbf{u} = 0, \tag{1}$$

$$\rho \frac{\mathrm{D}\mathbf{u}}{\mathrm{D}t} = -\nabla p + \eta_\mathrm{s} \nabla^2 \mathbf{u} + \nabla \cdot \boldsymbol{\tau}_\mathrm{p}, \tag{2}$$

$$\boldsymbol{\tau}_\mathrm{p} + \lambda \overset{\nabla}{\boldsymbol{\tau}}_\mathrm{p} + \alpha \frac{\lambda}{\eta_\mathrm{a}} \left(\boldsymbol{\tau}_\mathrm{p} \cdot \boldsymbol{\tau}_\mathrm{p} \right) = \eta_\mathrm{a} \left(\nabla \mathbf{u} + \nabla \mathbf{u}^\mathrm{T} \right), \tag{3}$$

$$\rho \frac{\mathrm{D}T}{\mathrm{D}t} = a \nabla^2 T, \tag{4}$$

with t the time, ρ the fluid density, η_s the Newtonian-solvent viscosity, λ the relaxation time, α the mobility factor, η_a the additive contribution to the zero-shear-rate solution viscosity ($\eta_0 = \eta_\mathrm{s} + \eta_\mathrm{a}$), and a the thermal diffusivity. These fluid properties are assumed to be constant, irrespective of the flow and the temperature fields. Equation (3) is the constitutive equation for viscoelastic fluid, which was first proposed by Giesekus (1982). The second term in the left-hand side of the equation expresses the the upper convected derivative. Among several variations of the non-Newtonian fluid model, we adopted this Giesekus model to properly resolve the evolution of extra stress due to the deformation of macromolecules in the surfactant solution. This

model is known to provide a reasonable description of the elongational viscosity (Bird, 1995) and one can find some reports demonstrating that measured rheological properties of the surfactant solution agree well with those of a Giesekus fluid (Suzuki *et al.*, 2001; Kawaguchi *et al.*, 2003). In order to mimic the solid body of the orifice in the fluid flow, the direct-forcing immersed boundary method described in detail by Fadlun *et al.* (2000) is applied on/inside the ribs on each side of the channel. To describe the system in a non-dimensional form, let us introduce a dimensionless conformation tensor $\mathbf{c} = c_{ij}$ given by an explicit function:

$$\boldsymbol{\tau}_{\mathrm{p}} = \frac{\eta_{\mathrm{a}}}{\lambda}\left(\mathbf{c} - \mathbf{I}\right). \tag{5}$$

The temperature T can be decomposed into the linear temperature (of the laminar solution for the smooth plane channel flow) and the fluctuation θ, and it can be made dimensionless by normalizing with the temperature difference between the channel:

$$\theta^* = \frac{1}{\Delta T}\left(T - \frac{\Delta T}{2\delta}y\right). \tag{6}$$

Then, the governing equations of Equations (2)–(4) may be written in dimensionless form as follows:

$$\begin{aligned} &\frac{\partial u_i^+}{\partial t^*} + u_j^+\frac{\partial u_i^+}{\partial x_j^*} \\ &= -\frac{\partial p^+}{\partial x_i^*} + \frac{\beta}{\mathrm{Re}_\tau}\frac{\partial^2 u_i^+}{\partial x_j^{*2}} + \frac{1-\beta}{\mathrm{We}_\tau}\frac{\partial c_{ij}}{\partial x_j^*} + F_i, \end{aligned} \tag{7}$$

$$\begin{aligned} &\frac{\partial c_{ij}}{\partial t^*} + u_k^+\frac{\partial c_{ij}}{\partial x_k^*} - \frac{\partial u_i^+}{\partial x_k^*}c_{kj} - c_{ik}\frac{\partial u_j^+}{\partial x_k^*} \\ &\quad + \frac{1}{\lambda}\left[c_{ij} - \delta_{ij} + \alpha\left(c_{ik} - \delta_{ik}\right)\left(c_{kj} - \delta_{kj}\right)\right] = 0, \end{aligned} \tag{8}$$

and

$$\frac{\partial \theta^*}{\partial t^*} + u_j^+\frac{\partial \theta^*}{\partial x_j^*} = \frac{1}{\mathrm{Pr}\,\mathrm{Re}_\tau}\frac{\partial^2 \theta^*}{\partial x_j^{*2}} - \frac{v^+}{2}. \tag{9}$$

The last term on the right-hand side of Equation (9) is derived from the non-linear term in Equation (4), and v is the wall-normal instant velocity. Quantities with a superscript of $(^+)$ indicate that they are normalized by $u_{\tau 0}$, which is given by the force balance between the wall shear stress and

the mean pressure gradient through the computational volume in the case of the plane channel without the orifice, i.e.,

$$u_{\tau 0} = \sqrt{\frac{\tau_{\mathrm{w}0}}{\rho}} = \sqrt{-\frac{\delta}{\rho} \cdot \frac{\Delta p}{L_x}}. \tag{10}$$

Here, $\tau_{\mathrm{w}0}$ is the wall shear stress in the case of the smooth plane channel flow and Δp is the time-averaged pressure drop between $x = -L_x/2$ and $L_x/2$. The superscript of $(^*)$ represents non-dimensionalization by the channel half width: e.g., $x^* = x/\delta$. The viscosity ratio $\beta = \eta_{\mathrm{s}}/\eta_0$ in Equation (7) is the ratio of the solvent viscosity to the solution viscosity at a state of zero shear stress. The additional term of F_i in Equation (7) represents the body force vector per unit volume for the immersed boundary method.

For the spatial discretization, the finite difference method is adopted. The central scheme with the 4th-order accuracy is employed in the x and z directions, and 2nd-order accuracy is applied in the y direction. The MINMOD scheme (a flux-limiter scheme) is adapted to the convective term in Equation (8): details of this numerical method can be found in Yu and Kawaguchi (2004). Time advancement is carried out by the 3rd-order Runge-Kutta method, but the 2nd-order Crank-Nicolson method is used for the viscous term in the y direction.

We executed two simulations of a viscoelastic-fluid flow and a Newtonian-fluid flow for comparison. The friction Reynolds number defined as $\mathrm{Re}_\tau = \rho u_\tau \delta/\eta_0$ was fixed at 200 for each simulation. The Weissenberg number representing the ratio between the relaxation time and the viscous time scale was chosen to be $\mathrm{We}_\tau = \rho\lambda u_{\tau 0}^2/\eta_0 = 20$. The other constant parameters were taken as $\alpha = 0.001$, $\beta = 0.8$, and the Prandtl number $Pr = \eta_0/(\rho a) = 1.0$. These rheological conditions would provide a noticeable drag-reducing effect to turbulent flows in a smooth channel. One may know that actual viscoelastic liquids and their drag-reducing effect would strongly depend on the temperature: see, for instance, Li *et al.* (2004), who reported an existence of the upper critical temperature, over which the flow lost the effectiveness of DR and HTR. The temperature dependency is more complicated that those for the Newtonian fluid, and itself depends on the kind of additive polymer or surfactant and on the absolute temperature. In this study, we consider the case of a small temperature difference, that does not change the fluid properties. As for the Newtonian-fluid calculation, $\mathrm{We}_\tau = 0$ and $\beta = 1$. Two different grids of $256 \times 128 \times 256$ and $128 \times 128 \times 128$ in (x, y, z) were used for the Newtonian and the viscoelastic fluid flows, respectively. In the

wall-normal direction, the density of the computational mesh is not uniform and becomes high at the height of the orifice rib and near the walls.

3. Result and Discussion

3.1. Drag and heat-transfer reduction rates

The drag coefficient and the globally averaged Nusselt number in the present study are defined as

$$f = \frac{\Delta p}{L_x} \cdot \frac{\delta}{\frac{1}{2}\rho U_{\mathrm{m}}^2} = \frac{2}{U_{\mathrm{m}}^{+2}}, \tag{11}$$

where $U_{\mathrm{m}} = 0.5 \int_0^2 \overline{u}\, \mathrm{d}y^*$ is the bulk mean velocity, and

$$\mathrm{Nu} = 4\frac{\partial \overline{T}^*}{\partial y^*}, \tag{12}$$

respectively. Note that the drag coefficient contains the form drag by the orifice and the frictional drag on the wall surfaces. An overbar denotes an averaged value with respect to time and the spanwise direction. The drag-reduction rate and the heat transfer reduction rate are generally defined as follows,

$$DR\% = \frac{f_{\mathrm{Newt}} - f_{\mathrm{VE}}}{f_{\mathrm{Newt}}} \times 100(\%), \tag{13}$$

$$HTR\% = \frac{\mathrm{Nu}_{\mathrm{Newt}} - \mathrm{Nu}_{\mathrm{VE}}}{\mathrm{Nu}_{\mathrm{Newt}}} \times 100(\%), \tag{14}$$

where the suffixes 'Newt' and 'VE' stand for values in the Newtonian flow and the viscoelastic flow, respectively. In Equation (14), the Nusselt number is averaged along the streamwise direction, except for the orifice position. The presently obtained values are $DR\% = 15\%$ and $HTR\% = 5.4\%$, indicating that the present viscoelastic fluid provides attenuation of the drag and the heat transfer. The bulk Reynolds number is increased from $\mathrm{Re}_{\mathrm{m}} = 2u_{\mathrm{m}}\delta/\eta_0 = 1100$ in the Newtonian case to 1200 in the viscoelastic flow, while the pumping pressure is the same in both cases. It was found that the drag reduction rate was much larger than the heat transfer reduction rate and this ratio ($DR\%/HTR\%$) was about 2.8. As for the smooth channel flow, Tsukahara and Kawaguchi (2011b) reported that this ratio varied in a small range of 0.9 to 1.1 among the different Weissenberg numbers, and that the similarity between the momentum transfer and the heat transfer was maintained even in drag-reduced turbulent flows. In the present flow configuration with the

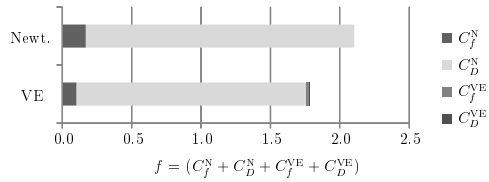

Figure 2: Decomposition of drag coefficient.

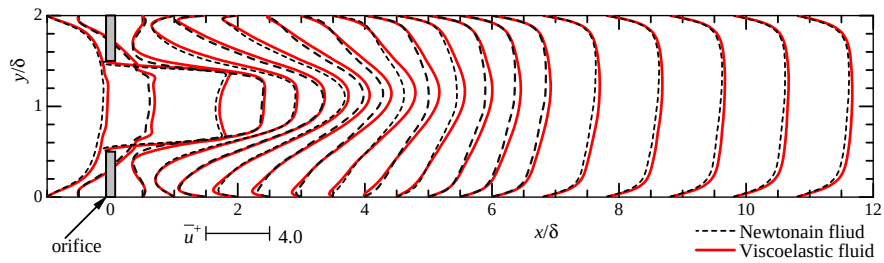

Figure 3: Mean streamwise velocity profiles at different streamwise positions.

orifice, this relationship has collapsed, that is, in the viscoelastic fluid the drag is more suppressed compared with the heat-transfer rate.

The total drag of f can be decomposed into four components:

$$f = C_D^{\mathrm{N}} + C_f^{\mathrm{N}} + C_D^{\mathrm{VE}} + C_f^{\mathrm{VE}}, \tag{15}$$

$$C_D^{\mathrm{N}} = \frac{1}{u_{\mathrm{m}}^{+2}} \int_S \overline{p}^+ \left(\mathbf{e}_x \cdot \mathbf{n}\right) \mathrm{d}S^*, \tag{16}$$

$$C_f^{\mathrm{N}} = \frac{1}{u_{\mathrm{m}}^{+2}} \frac{\beta}{\mathrm{Re}_\tau} \int_S \frac{\partial \overline{u}^+}{\partial y^*} \left(\mathbf{e}_y \cdot \mathbf{n}\right) \mathrm{d}S^*, \tag{17}$$

$$C_D^{\mathrm{VE}} = \frac{1}{u_{\mathrm{m}}^{+2}} \frac{1-\beta}{\mathrm{We}_\tau} \int_S \overline{c_{xx}} \left(\mathbf{e}_x \cdot \mathbf{n}\right) \mathrm{d}S^*, \tag{18}$$

$$C_f^{\mathrm{VE}} = \frac{1}{u_{\mathrm{m}}^{+2}} \frac{1-\beta}{\mathrm{We}_\tau} \int_S \overline{c_{xy}} \left(\mathbf{e}_y \cdot \mathbf{n}\right) \mathrm{d}S^*, \tag{19}$$

where S represents all the wall surface including the orifice surface, $\mathbf{e}_i$ the unit vector, and $\mathbf{n}$ the rib surface normal vector. Each component of C_D^{N}, C_f^{N}, C_D^{VE}, and C_f^{VE} means the form drag, the frictional drag (containing the turbulent frictional drag), the c_{xx} (normal stress) contribution term, and the

c_{xy} (shear stress) contribution term, respectively, and their partition ratio with respect to f is shown in Figure 2. The last two terms appears only in the viscoelastic case. As can easily be seen from the figure, the form drag by the orifice is dominant and the summation of the other terms is less than 10% of the total. The value of C_D^{N} for the viscoelastic fluid is reduced by 15% of that for the Newtonian fluid: in fact, the level of $DR\%$ in the present viscoelastic flow is comparable to this reduction of C_D^{N}. This implies that the drag reduction in the present study can be attributed to modulation of the mean flow pattern around the orifice rather than of turbulent motions. In the case of a smooth channel without obstacles, only the reduction in the Reynolds shear stress is responsible for the drag reduction. Actually, the magnitude of C_f^{N} decreases by 40% of the Newtonian value. However, this frictional drag reduction is less significant, because the pressure drop due to the orifice is large compared to that caused by the friction and, in addition, the extra forces (C_D^{VE} and C_f^{VE}) by the elasticity in the non-Newtonian case apparently compensate for the diminution of C_f^{N}.

Figure 3 shows the ensemble averaged streamwise velocity profiles at different streamwise positions along the channel. The profile of the viscoelastic flow reveals an increase in the quantity of high-momentum fluid in the channel central region passing by the orifice. This is because the turbulent momentum transfer is less significant relative to the Newtonian case. Thereby, the mean velocity of the near-wall fluid, which should impinge upon the orifice face, becomes small and the momentum loss might be avoided more or less in the present viscoelastic flow. Moreover, by the careful observation of the expanding flow past the orifice, the strong shear layer separating from the orifice edge for the viscoelastic flow seems to extend further towards each wall, compared to the Newtonian case. Observing Figure 4, where streamlines based on the time-averaged mean velocity are given for each flow, it appears clearly that the streamlines in the high-speed core flow of the viscoelastic

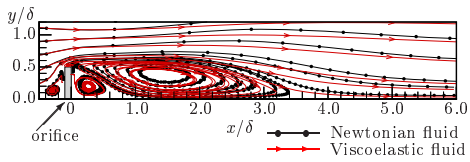

Figure 4: Comparison of mean streamline patterns with empahsis on the recirculation zone behind the lower orifice rib.

fluid deviate from those of the Newtonian fluid, especially for $x/\delta = 1$–5, and approach the wall. Therefore, the spacing of streamlines becomes wider in the viscoelastic flow. This suggests swelling behavior at the expansion, the so-called 'Barus effect': see, for example, Bagley and Duffey (1970). This effect is well-known to be related to the difference in primary normal stresses due to the fluid elasticity. As a consequence of the swelling flow, the recirculation zone just behind the orifice is thinner, as seen in Figure 4, and the weakening of pressure inside the zone is moderated, resulting in a reduction of C_D^{N}.

Despite the thinning of recirculation zone, the reattachment length was found to increase from $x/\delta = 3.8$ to 4.3 in the viscoelastic fluids, although cannot be clearly seen from Figure 4. This is qualitatively consistent with the observations made by Pak *et al.* (1990) and other researchers, who reported from their parametric experiments that the reattachment length for the viscoelastic liquids was a 2–3 times longer than those for water, and gradually increased with increasing concentration of viscoelastic solutions. They mentioned that the shifted reattachment should be caused by the fact that the fluid elasticity suppressed the eddy motion which would extend the region of the recirculation zone.

Since the present system of the channel with a rectangular orifice involves a sudden contraction and expansion, the characteristics of turbulence change in a streamwise direction. Therefore, the local friction factor and the local Nusselt number are evaluated, as shown in Figures 5 and 6. In the Newtonian flow, these values of C_f^{N} and Nu are different between the lower and upper walls, because the mean flow bends toward either the upper or lower side walls, and thus the flow field becomes asymmetric along the channel center. Such a phenomenon in symmetric sudden expansion flows has been previously reported in the literature (see, for instance, Cherdron *et al.*, 1978; Oliveira, 2003; Makino *et al.*, 2008a), and is known to be caused by the Coanda effect. It should be noted that the results shown in this paper are of the case where the mean flow bends to the upper side, but also note that, in theory, the direction of bending is determined randomly, with equal probability for either direction. The reattachment point can be identified as the position where $C_f^{\mathrm{N}} = 0$. As seen in Figure 5, the reattachment points on the upper and lower walls are disaccord, especially, in the Newtonian flow. While the point on the lower wall is confirmed to be shifted downstream in the viscoelastic flow, that on the upper wall remains stationary at around $x = 3\delta$ from the orifice. In the region between the orifice and the reattachment point, the local

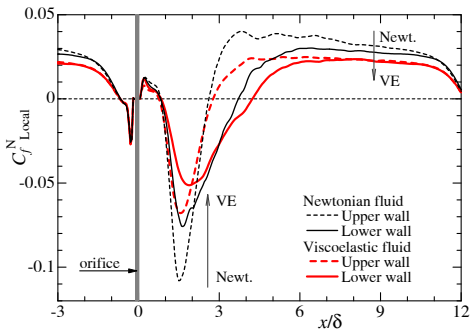

Figure 5: Streamwise distribution of local frictional coefficient.

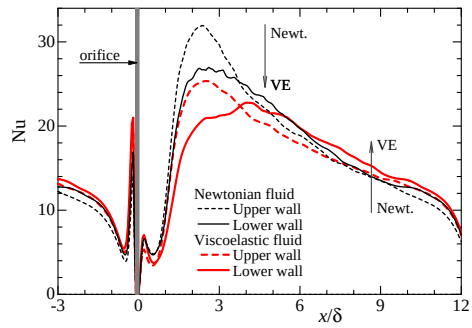

Figure 6: Streamwise distribution of local Nusselt number.

C_f^{N} reveals negative values, implying the existence of a recirculation zone. In this region, both $C_{f\ \mathrm{Local}}^{\mathrm{N}}$ and Nu are suppressed in the viscoelastic flow. This might be due to the suppression of eddies which are generated at the top of the orifice due to Kelvin-Helmholtz instability, as discussed in Section 3.2. The magnitude of the negative peak of $C_{f\ \mathrm{Local}}^{\mathrm{N}}$ on the upper wall at $x = 1.5\delta$ is reduced by 37%, whereas that of the Nusselt number is only reduced by 15%. On the other hand, in the region behind the reattachment point, the friction is suppressed, but interestingly the heat transfer is maintained or enhanced, especially, in $x > 6.0\delta$, for the viscoelastic flow compared to the Newtonian flow, i.e., local $\mathrm{Nu}_{\mathrm{Newt}} <$ local $\mathrm{Nu}_{\mathrm{VE}}$. We may presume that this paradoxical phenomenon, the heat transfer enhancement in the drag-reduced viscoelastic flow, is caused by turbulent structures. Quasi-streamwise vortical structures are dominant far downstream from the orifice, and these vortices induce mixing of fluid and heat in the near-wall region. The quasi-streamwise

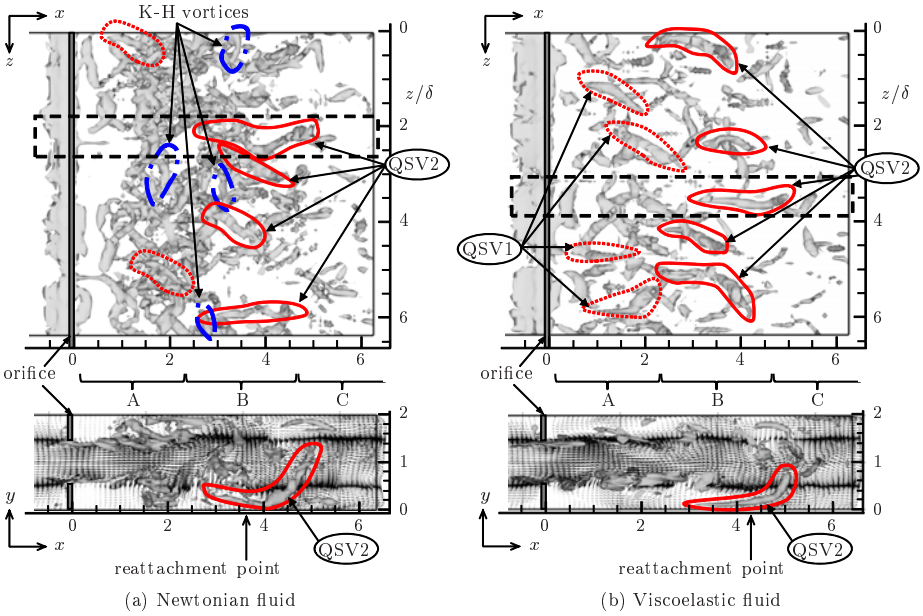

Figure 7: Vortex structures visualized by the iso-surface of the second invariant of the velocity gradient tensor, $Q^+ < -0.01$, in the downstream region of the orifice. The top figure shows the top view from the y direction, and the bottom shows the side view from the z direction. A vortex enclosed by a red solid line is a quasi-streamwise vortex around the reattachment point (labeled as QSV2); a red dashed line is a quasi-streamwise vortex (QSV1) above the recirculaton region near the orifice (see region-A); and the blue chain line is a K-H vortex in region-B. Dashed-line boxes in top figures show the visualized fields in respective bottom figures.

vortices are found to be maintained further in the viscoelastic flow. Details about these vortical structures are discussed in the following.

3.2. Relation between vortex structure and heat fluctuation

Figure 7 shows visualization of vortical structures in each flow field with emphasis on the downstream of the orifice, where a vortex is identified by the iso-surface of the second invariant of the velocity-deformation tensor, defined as

$$Q^+ = -\frac{\partial u_i^+}{\partial x_j^+}\frac{\partial u_j^+}{\partial x_i^+}. \tag{20}$$

As observed in Figure 7(b), spanwise vortices parallel to the orifice, which may be regarded as the Kelvin-Helmholtz (K-H) vortices, are found to be

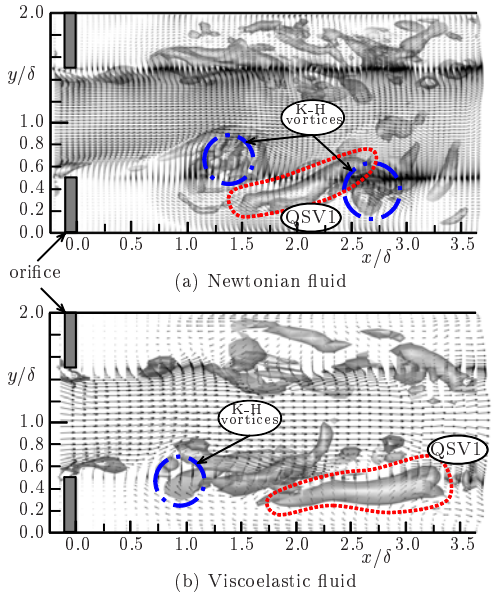

Figure 8: Enclosed side view of quasi-streamwise vortex (QSV1) with emphasis on the area just behind the orifice.

suppressed in the viscoelastic flow, while the quasi-streamwise vortices (QSV) are found around and downstream of the reattachment point, similar to those in the Newtonian flow. Therefore, the Reynolds stress and also the drag coefficient were decreased locally just behind the orifice, as shown in Figure 5. On the other hand, in the region behind the reattachment point, the quasi-streamwise vortices (labeled as QSV2 in the figure) have large-scale features and reach the channel central region. It seems that these streamwise vortices are dominant and enhance the turbulent heat transfer in this area, i.e., region B in Figure 7).

Figure 8 shows details of QSV1, which are located in the region around the orifice height and between the K-H vortices. This vortex structure seems to bridge a sequence of the spanwise K-H vortices. Let us recall that Hussain (1986) and Comte *et al.* (1992) performed DNS of mixing layers and they reported similar vortex patterns in the form of vortex-lattice structures. In the Newtonian flow, this vortex pattern can be found, but in the viscoelastic fluid the (spanwise) K-H vortices decayed rapidly in the downstream region. This must be because small eddies as well as the K-H vortices can be damped

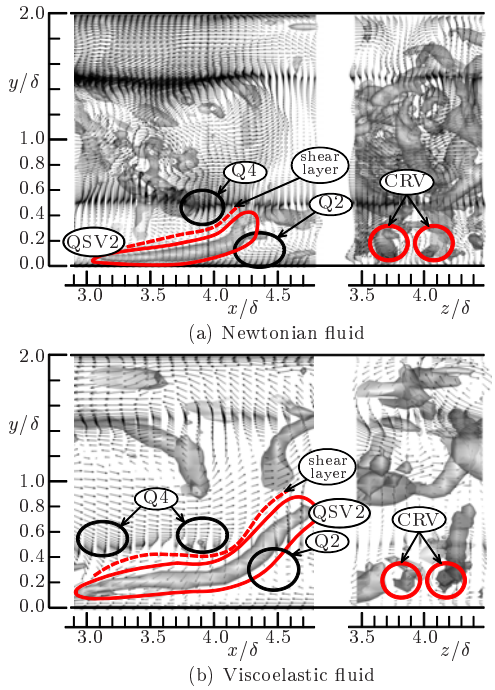

Figure 9: Enclosed side view of quasi-streamwise vortex (QSV2) with emphasis on the area around the reattachment point. The abbreviations used here are: Q2, ejection; Q4, sweep; and CRV, counter-rotaing vortex pairs.

by the fluid elasticity with a longer relaxation time relative to time scales of their turbulent eddies. After an initial growth in the shear layer emanating from the orifice edge, the QSV1 is advected downstream and toward the wall surface, and then it might be regarded as QSV2. Figure 9 again focuses on the streamwise vortex of QSV2 around the reattachment point. This vortex is similar to the hairpin vortex observed in the turbulent boundary layer, but the head of the hairpin vortex cannot be found. The ejection (Q2 event) and sweep (Q4) motions can be observed under and above the vortex, respectively, and it seems that these motions enhance the heat transfer. If viewed from the streamwise direction, the counter-rotating pair of vortices (CRV) can be found to occur as the same with the legs of the hairpin vortex (cf., Robinson, 1991).

Figure 10 shows the time advancement of the vortical structures in the bottom half of the channel to observe the temporal variation of quasi-streamwise

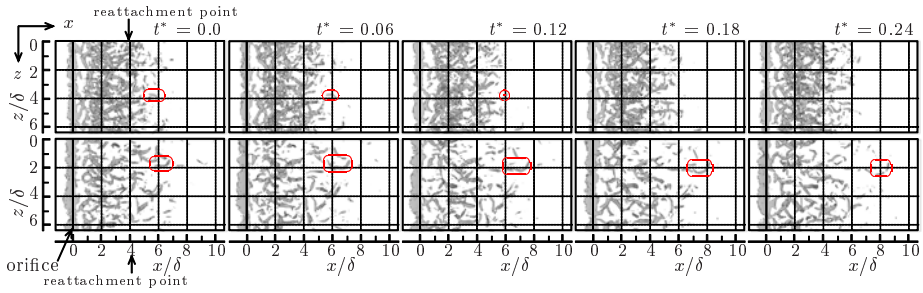

Figure 10: Time advancement of vortical structures in the lower half of the channel, viewed from the top. Top, Newtonian fluid; bottom, viscoelastic fluid. The region enclosed by a red line is a quasi-streamwise vortex.

vortices. The quasi-streamwise vortices are propagated downstream by the main flow. In the viscoelastic flow, the quasi-streamwise vortex (enclosed by a red line in the figure) is maintained for a longer time compared to those observed in the Newtonian flow, and carried further downstream. As is well known, energy-containing large-scale eddies in turbulence should be broken into smaller eddies and this energy cascade would be ended up at the dissipation Kolmogorov scale (Tennekes and Lumley, 1972). In the drag-reducing viscoelastic fluid, the dissipative scale is basically expected to be increased up to the scale relevant to the relaxation time. If energy is inhibited from cascading into smaller eddies in that manner, large-scale eddies should dissipate by viscous dissipation, taking a long time relevant to their time scale. Therefore, the quasi-streamwise vortices, which are relatively large compared to the turbulent eddies in a Newtonian flow, would survive for a longer time period. Moreover, we previously proposed a sustenance mechanism of quasi-streamwise vortex, that is, turbulent kinetic energy is transferred to the elastic energy of the fluid through the K-H vortex suppression, and the adverse exchange from the elastic to the kinetic energy occurs apart from the orifice (Tsukahara *et al.*, 2011e). Then it may be concluded that those long-life vortices would enhance the turbulent heat transfer in a remote area away from the orifice. Consequently, the present ribbed channel would contribute to heat-transfer enhancement behind the reattachment point.

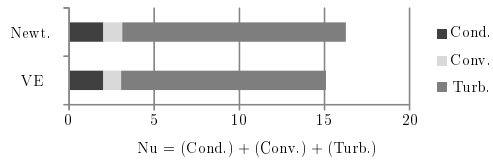

Figure 11: Decomposition of Nusselt number.

3.3. Turbulent heat flux

To examine the contribution of the mean flow and the turbulent fluctuation to the heat-transfer rate, a mathematical relation is derived with reference to Fukagata *et al.* (2002, 2005). The Nusselt number can be decomposed to several terms as in this equation:

$$\mathrm{Nu} = 2 + 2\mathrm{Re_m}\mathrm{Pr}\int_V \left[\left(-\overline{v}^*\overline{\theta}^*\right) + \left(-\overline{v'^*\theta'^*}\right)\right] \mathrm{d}V, \tag{21}$$

where the first, second, and third terms represent the heat conduction term, the convective heat-transfer term, and the turbulent heat transfer term, respectively. Here, v^* is nondimensionalized by twice the bulk mean velocity $2U_\mathrm{m}$, and the prime notation ($'$) represents the fluctuating component. The heat flux from the orifice surface was ignored when this equation was derived, because the orifice volume is small enough relative to the computational domain size. The streamwise turbulent heat flux is absent because of the periodicity in the streamwise direction. Each term of Equation (21) is shown in Figure 11 for both the Newtonian and the viscoelastic flows. It has been confirmed that the value of Nu calculated from Equation (12) agrees well with the directly calculated value by Equation (21) with an accuracy of 3%. At the present Reynolds number, the convective heat transfer by the mean flow is less significant than the contribution of turbulence. Therefore, almost all heat transfer is generated by the wall-normal turbulent heat flux, and it seems that the quasi-streamwise vortex around the reattachment point plays a key role in producing this heat flux.

Figures 12 and 13 show respectively the wall-normal and streamwise turbulent heat fluxes, $-\overline{v'^*\theta'^*}$ and $\overline{u'^*\theta'^*}$, at different streamwise positions. In the present system, the constant temperature difference is adopted for the thermal boundary condition, and thus $-\overline{v'^*\theta'^*}$ strongly contributes to the heat transfer throughout the channel. In the viscoelastic flow, $\overline{u'^*\theta'^*}$ in the separated shear layer, which is induced by the orifice, is larger than that

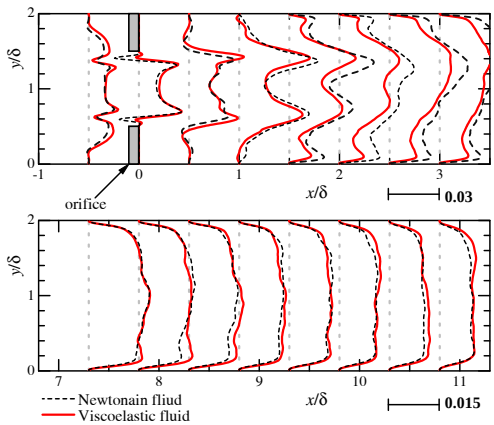

Figure 12: Wall-normal turbulent heat flux, around (top) and the far downstream (bottom) of the orifice.

for the Newtonian flow. Therefore, this term encourages heat transfer in a streamwise direction. On the other hand, $-\overline{v'^*\theta'^*}$ is suppressed in this region because the reduction of the spanwise vortices causes a reduction of the heat exchange between the channel center and the recirculation zone. In the region of $x = 6.3$–10.3, $-\overline{v'^*\theta'^*}$ becomes larger than that in the Newtonian flow. This indicates that maintaining the quasi-streamwise vortices causes the heat transfer enhancement, as mentioned in the previous section. Here, the mean turbulent heat flux may be expressed as

$$-\overline{v'\theta'} = R_{v\theta} v'_{\mathrm{rms}} \theta'_{\mathrm{rms}}, \tag{22}$$

where $R_{v\theta}$ is the cross-correlation coefficient between the wall-normal velocity fluctuation v' and the temperature fluctuation θ'. The profiles of $R_{v\theta}$ and the root-mean-square values of v' and θ' are shown in Figure 14. In the viscoelastic flow, $-\overline{v'^*\theta'^*}$ is suppressed in the region behind the orifice, as previously mentioned, but $R_{v\theta}$ and θ_{rms} are almost unchanged between both fluids. Hence, the reason for the suppression of $-\overline{v'^*\theta'^*}$ is only the suppression of the v'^+_{rms}: in other words, the Nusselt number is significantly influenced by the turbulent structure in the velocity field. The reduction for v'^+_{rms} seen at $x/\delta = 0.5$ persists as far as $x/\delta = 5$, and its peak decent is as much as 20% compared to the Newtonian case. This result agrees well with the experiments on a backward-facing step flow (Poole and Escudier, 2003a) and an axisymmetric sudden-expansion pipe flow (Poole and Escudier, 2003b, 2004) of viscoelastic liquids. In addition, Poole and Escudier (2004) found

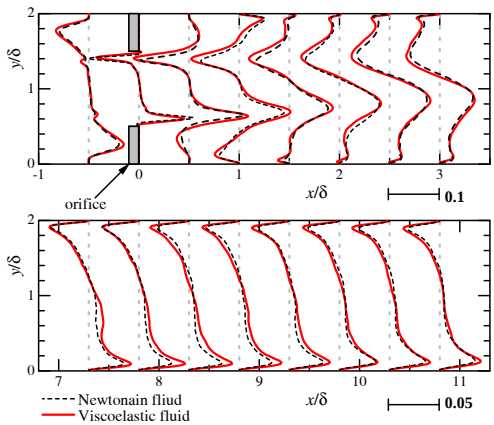

Figure 13: Streamwise turbulent heat flux, around (top) and the far downstream (bottom) of the orifice.

that the v'_{rms} exceed the Newtonian values in a limited area in the high-velocity core between 5–8 step heights downstream, but note that their area-expansion ratios were different from the present. Similarly, our present result indicates a slight increase of v'^{+}_{rms} in the viscoelastic fluid from $x/\delta = 6$.

A typical distribution of the temperature fluctuation in the x-y plane at an arbitrary z position is shown in Figure 15. In the region (highlighted by a dotted box) far downstream from the reattachment point, the temperature fluctuations have striped pattern (marked by circles in the figure) inclined against the streamwise direction—they seem to be raised gradually from the wall surface. Each stripe pattern is caused by a longitudinal vortex of QSV2 (as those presented in Figure 7), that has been advected further from the orifice and approaches a next orifice in the downstream. (Note again that we imposed the periodic boundary conditions at the upstream and downstream boundaries, and hence the approaching flow in the upstream of the orifice may be regarded as the downstream flow past another orifice located upstream by $L_x = 12.8\delta$: for instance, the field at $x/\delta = -4$ corresponds to that at $x/\delta = 8.8$.) The longitudinal vortex has an ejecting motion, by which near-bottom-wall cold fluid is lifted up toward the channel center, so the striped pattern is formed and $\theta'^{+}_{\mathrm{rms}}$ has a peak near the wall in this region: see Figure 14(c). These stripes have almost the same features in the two fluids, in terms of size and magnitude. Thus the $\theta'^{+}_{\mathrm{rms}}$ profiles are virtually identical for these fluid flows. It is consistent with the result of the local Nusselt

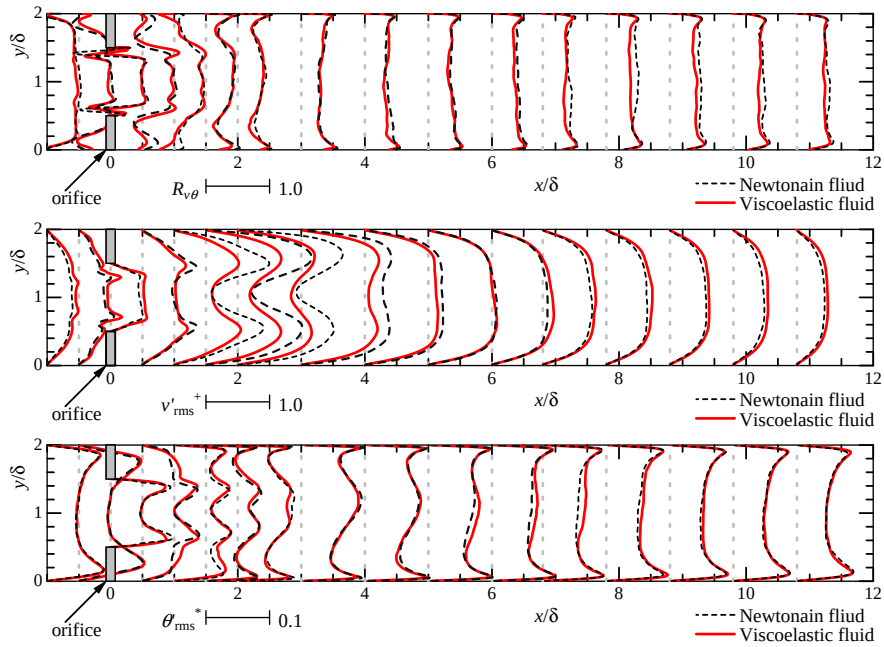

Figure 14: Cross-correlation coefficient $R_{v\theta}$, wall-normal turbulent intensity v'^{+}_{rms}, and temperature variance $\theta'^{+}_{\mathrm{rms}}$, from top to bottom figures.

number (see Figure 6), which shows less dependence on fluid in this area. Precisely speaking as far as the area of $x/\delta = 6$–9, the vortex motions and temperature fluctuations are slightly stronger in the case of the viscoelastic fluid, and thereby the local Nusselt number for the viscoelastic fluid outweigh that for the Newtonian fluid.

In the core region behind the orifice, although the temperature distribution exhibits fine-scale fluctuations in the Newtonian flow compared to the viscoelastic flow as shown in Figure 15, the profiles of $\theta'^{+}_{\mathrm{rms}}$ reveal the same irrespective of the different fluid in Figure 14(c). In this region, the temperature fluctuation has a large-scale structure, which stretches from the near-wall region just in front of the orifice to the core region behind the orifice. It seems that this structure contributes to the peak of the $\theta'^{+}_{\mathrm{rms}}$ profile around the orifice height. This large-scale structure observed in the temperature field comes intermittently from the near-wall striped structure approaching the orifice. Therefore, the decay of the K-H vortices has an insignificant effect on the peak of the $\theta'^{+}_{\mathrm{rms}}$ profile behind the orifice, while the magnitude of v'_{rms}

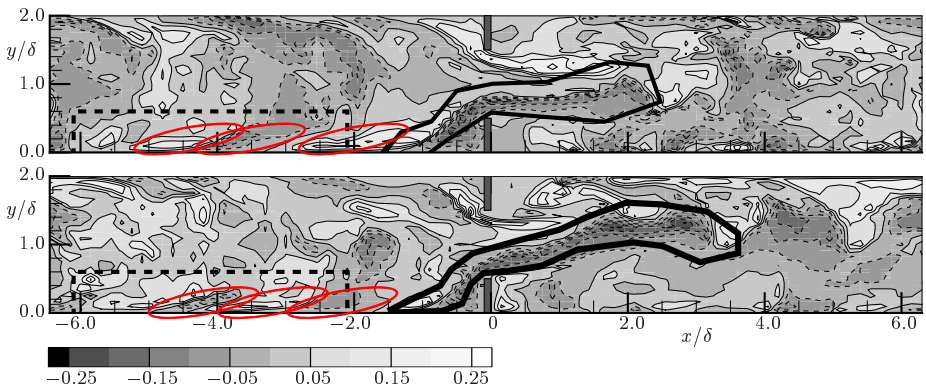

Figure 15: Typical distribution of instantaneous temperature fluctuation, θ'^*. The solid contours denote $\theta' \geq 0$, and dashed contours denote $\theta' < 0$. The contour increment is $0.05\Delta T$. Top, Newtonian fluid; bottom, viscoelastic fluid. The solid lines of red and black enclose the striped structure and the large-scale structure around the orifice, respectively.

is greatly decreased by the weakening of spanwise vortices at the position. A reason for explicit appearance of the large-scale structure in the thermal field is non-zero mean temperature gradient ($\partial T/\partial y \neq 0$) in the core region. Comparing the instantaneous fields given in Figure 15 may imply that the large-scale structure observed in the viscoelastic fluid should elongate further downstream. Moreover, one can discern some traces of large-scale temperature fluctuations in the area of $x/\delta = 4$–7 in (b). Presumably this difference from the Newtonian case should be attributed to the absence of strong mixing (or the turbulent diffusion) by the K-H vortices in the orifice downstream.

4. Conclusions

We performed direct numerical simulations of turbulent heat transfer in a viscoelastic fluid flow through a channel with periodic rectangular orifices at streamwise intervals of 12.8δ, and presented several statistics regarding the velocity and thermal fields. In this study, we neglected the temperature dependence of the fluid and rheological properties. The most important conclusion drawn from this research is that the dissimilarity between the velocity and thermal fields was remarkable due to the orifice in the context of the reductions in drag and heat transfer, even under the condition of

Pr = 1.

In the present condition ($\mathrm{Re}_\tau = 200$, $\mathrm{We}_\tau = 20$, and $\beta = 0.8$), the obtained drag-reduction rate was 15%, while the heat-transfer reduction rate was 5.4%. The drag reduction was caused mainly by a reduction in the form drag, and the heat-transfer reduction was caused by the turbulent heat-transfer reduction. The heat-transfer reduction effect was not remarkable compared with that in the smooth channel flow. This was due to the sustainment of quasi-streamwise vortices behind the reattachment point in the viscoelastic flow. The wall-normal turbulent heat flux in this region became larger in the viscoelastic flow than in the Newtonian flow. Accordingly, the heat transfer was locally enhanced downstream of the reattachment point in the viscoelastic flow. On the other hand, the elasticity exerted a suppresing effect on turbulent motions in the strong shear layer emanating from the orifice edge, where the spanwise vorticities due to the Kelvin-Helmholtz instability were decayed rapidly in the viscoelastic flow. This resulted in the decrease of both the local skin friction and the local Nusselt number in the recirculation zone below the shear layer.

For the demonstration of developed flow in a long channel with regularly spaced orifice elements, we employed the periodic condition for the streamwise boundaries of the domain, in which a single orifice was installed. This boundary condition should affect more or less the results shown above, but a sufficiently long computational domain is expected to allow us to make no account of the artificial influence. Actually, the streamwise length of the present domain was long enough to capture the turbulent eddies as confirmed by the flow visualizations. Although the near-wall streaky structures are known to elongate in drag-reducing fluid, we have observed no structure extending throughout the domain in this study. The presence of orifices might lead to inhibition of elongation of flow structures. Moreover, the influence of the periodic boundary on the mean flow is also insignificant in this study, since we make sure that the approaching flow at the the orifice upstream is symmetric about the centerline, at least statistically: see Figures 3 and 12–14. By extending the streamwise length of the domain with a single orifice, that is equivalent to widening of the orifice interval, the ratio of the reduction rates in drag and heat transfer ($DR\%/HTR\% = 2.8$) would approach 1.0 as obtained in the smooth channel flow. In viscoelastic flows passing the sudden expansion, the reattachment length may be significantly affected by characteristics of the inlet turbulent flow, as Pak *et al.* (1990) and Poole and Escudier (2003a) already reported, and should be investigated in

the future.

Finally, the present Reynolds and Prandtl numbers are considerably lower than those in practical flow systems. The above conclusions have been drawn from limited cases, however similar experimental studies are in progress and the difference between the present flows and real flows will be examined.

Acknowledgements

The present computations were performed with the use of supercomputing resources of Cyberscience Center at Tohoku University, and of the Earth-Simulator Center of JAMSTEC (Japan Agency for Marine-Earth Science and Technology).

References

Bagley, E.B. and Duffey, H.J. (1970) 'Recoverable shear strain and the barus effect in polymer extrusion,' *Journal of Rheology*, Vol. 14, No. 4, pp. 545–553.

Bird, R.B. (1995) 'Constitutive equations for polymeric liquids,' *Annual Review of Fluid Mechanics*, Vol. 27, pp. 169–193.

Cai, W.H., Li, F.C., Zhang, H.N., Li, X.B. Yu, B., Wei, J.J., Kawaguchi, Y., and Hishida, K. (2009) 'Study on the characteristics of turbulent drag-reducing channel flow by particle image velocimetry combining with proper orthogonal decomposition analysis,' *Physics of Fluids*, Vol. 21, No. 11, 115103, 12 pp.

Cherdron, W., Durst, F., and Whitelaw, J.H. (1978) 'Asymmetric flows and instabilities in symmetric ducts with sudden expansions,' *Journal of Fluid Mechanics*, Vol. 84, pp. 13–31.

Comte, P., Lesieur, M., and Lamballais, E. (1992) 'Large- and small-scale stirring of vorticity and a passive scalar in a 3-D temporal mixing laye,' *Physics of Fluid A*, Vol. 4, No. 4, pp. 2761–2778.

Dimitropoulos, C.D., Sureshkumar, R.,Beris, A.N., and Handler, R.A. (2001) 'Budgets of Reynolds stress, kinetic energy and streamwise enstrophy in viscoelastic turbulent channel flow,' *Physics of Fluids*, Vol. 13, No. 4, pp. 1016–1027.

Fadlun, E.A., Verzicco, R., Orlandi, P., and Mohd-Yusof, J. (2000) 'Combined immersed boundary finite-difference methods for three-dimensional complex flow simulations,' *Journal of Computational Physics*, Vol. 161, No. 1, pp. 35–60.

Fukagata, K., Iwamoto, K., and Kasagi, N. (2002) 'Contribution of Reynolds stress distribution to the skin friction in wall-bounded flows,' *Physics of Fluids*, Vol. 14, No. 11, pp. L73–L76.

Fukagata, K., Iwamoto, K., and Kasagi, N. (2005) 'Novel turbulence control strategy for simultaneously achieving friction drag reduction and heat transfer augmentation,' *Proceedings of 4th International Symposium on Turbulence and Shear Flow Phenomena*, 27–29 June 2005, Williamsburg, USA, pp. 307–312.

Giesekus, H. (1982) 'A simple constitutive equation for polymer fluids based on the concept of deformation-dependent tensorial mobility,' *Journal of Non-Newtonian Fluid Mechanics*, Vol. 11, No. 1/2, pp. 69–109.

Gupta, V.K., Sureshkumar, R., and Khomami, B. (2005) 'Passive scalar transport in polymer drag-reduced turbulent channel flow,' *AIChE Journal*, Vol. 51, No. 7, pp. 1938–1950.

Hussain, A.K.M. (1986) 'Coherent structures and turbulence,' *Journal of Fluid Mechanics*, Vol. 173, pp. 306–356.

Kagawa, Y., Yu, B., Kawaguchi, Y., Kawamura, H., and Shiraishi, Y. (2008) 'Turbulent heat transfer of viscoelastic fluid flow accompanied by drag reduction with DNS analysis,' *Progress in Computational Fluid Dynamics*, Vol. 8, pp. 477–485.

Kawaguchi, Y., Wei, J.J., Yu, B., and Feng, Z.P. (2003) 'Rheological characterization of drag-reducing cationic surfactant solution—shear and elongational viscosities of dilute solutions,' *Proceedings of ASME/JSME 2003 4th Joint Fluids Summer Engineering Conference*, 6–10 July 2003, Honolulu, USA, pp. 721–728.

Li, F.C., Kawaguchi, Y., and Hishida, K. (2004) 'Investigation on the characteristics of turbulence transport for momentum and heat in a drag-reducing surfactant solution flow ,' *Physics of Fluids*, Vol. 16, No. 9, pp. 3281–3295.

Makino, S., Iwamoto, K., and Kawamura, H. (2008a) 'Turbulent structures and statistics in turbulent channel flow with two-dimensional slits,' *International Journal of Heat and Fluid Flow*, Vol. 29, No. 3, pp. 602–611.

Makino, S., Iwamoto, K., and Kawamura, H. (2008b) 'DNS of turbulent heat transfer through two-dimensional slits,' *Progress in Computational Fluid Dynamics*, Vol. 8, No. 7/8, pp. 397–405.

Motozawa, M., Ishitsuka, S., Iwamoto, K., Ando, H., Senda, T., and Kawaguchi, Y. (2012) 'Experimental investigation on turbulent structure of drag reducing channel flow with blowing polymer solution from the wall,' *Flow, Turbulence and Combustion*, Vol. 88, No. 1/2, pp. 121–141.

Oliveira, P.J. (2003) 'Asymmetric flows of viscoelastic fluids in symmetric planar expansion geometries,' *Journal of Non-Newtonian Fluid Mechanics*, Vol. 114, No. 1, pp. 33–63.

Pak, B., Cho, Y.I., and Choi, S.U.S. (1990) 'Separation and reattachment of non-newtonian fluid flows in a sudden expansion pipe,' *Journal of Non-Newtonian Fluid Mechanics*, Vol. 37, No. 2–3, pp. 175–199.

Poole, R.J. and Escudier, M.P. (2003a) 'Turbulent flow of non-Newtonian liquids over a backward-facing step: Part II. Viscoelastic and shear-thinning liquids,' *Journal of Non-Newtonian Fluid Mechanics*, Vol. 109, No. 2–3, pp. 193–230.

Poole, R.J. and Escudier, M.P. (2003b) 'Turbulent flow of a viscoelastic shear-thinning liquid through a plane sudden expansion of modest aspect ratio,' *Journal of Non-Newtonian Fluid Mechanics*, Vol. 112, No. 1, pp. 1–26.

Poole, R.J. and Escudier, M.P. (2004) 'Turbulent flow of viscoelastic liquids through an axisymmetric sudden expansion,' *Journal of Non-Newtonian Fluid Mechanics*, Vol. 117, No. 1, pp. 25–46.

Robinson, S.K. (1991) 'Coherent Motions in the Turbulent Boundary Layer,' *Annual Review of Fluid Mechanics*, Vol. 23, pp. 601–639.

Suzuki, H., Ishihara, K., and Usui, H. (2001) 'Numerical study on a drag reducing flow with surfactant additives,' *Proceedings of 3rd Pacific Rim Conference on Rheology*, 8–13 July 2001, Vancouver, Canada, Paper No. 019.

Tennekes, H. and Lumley, J.L. (1972) *A First Course in Turbulence*, The MIT Press, Cambridge.

Toms, B.A. (1948) 'Some observations on the flow of linear polymer solutions through straight tubes at large Reynolds numbers,' *Proceedings of First International Congress on Rheology*, North-Holland Publishing Co., Amsterdam, pp. 135–141.

Tsukahara, T., Ishigami, T., Yu, B., and Kawaguchi, Y., (2011a) 'DNS study on viscoelastic effect in drag-reduced turbulent channel flow,' *Journal of Turbulence*, Vol. 12, No. 13, pp. 1–25.

Tsukahara, T. and Kawaguchi, Y. (2011b) 'Comparison of heat-transfer reduction in drag-reduced turbulent channel flows with different fluid and thermal boundary conditions,' *Progress in Computational Fluid Dynamics*, Vol. 11, No. 3/4, pp. 216–226.

Tsukahara, T. and Kawaguchi, Y. (2011c) 'Turbulent heat transfer in drag-reducing channel flow of viscoelastic fluid,' *Evaporation, Condensation and Heat transfer* (ed., A. Ahsan), InTech, Rijeka, Croatia, pp. 375-400.

Tsukahara, T., Kawase, T., and Kawaguchi, Y. (2011d) 'DNS of viscoelastic turbulent channel flow with rectangular orifice at low Reynolds number,' *International Journal of Heat and Fluid Flow*, Vol. 32, No. 3, pp. 529–538.

Tsukahara, T., Kawase, T., and Kawaguchi, Y. (2011e) 'Numerical investigation of viscoelastic effects on turbulent flow past rectangular orifice,' *Proceedings of 22nd International Symposium on Transport Phenomena*, 8–11 November 2011, Delft, The Netherlands, Paper No. 129.

Wang, Y., Yu, B., Wu, X., Wei, J.J., Li, F.C., and Kawaguchi, Y. (2011) 'POD study on the mechanism of turbulent drag reduction and heat transfer reduction based on direct numerical simulation,' *Progress in Computational Fluid Dynamics*, Vol. 11, No. 3/4, pp. 149–159.

White, C.M. and Mungal, M.G. (2008) 'Mechanics and prediction of turbulent drag reduction with polymer Additives,' *Annual Review of Fluid Mechanics*, Vol. 40, pp. 235–256.

Yu, B. and Kawaguchi, Y. (2004) 'Direct numerical simulation of the viscoelastic drag-reducing flow: a faithful finite-difference method,' *Journal of Non-Newtonian Fluid Mech.*, Vol. 116, No. 2/3, pp. 431–466.

Yu, B. and Kawaguchi, Y. (2005) 'DNS of fully developed turbulent heat transfer of a viscoelastic drag-reducing flow,' *International Journal of Heat and Mass Transfer*, Vol. 48, pp. 4569–4578.